Nanotechnology Perceptions
ISSN 1660-6795
www.nano-ntp.com

Comparative Study of Strontium and Strontium Nitrate using Wavelength Dispersive X-ray Fluorescence

Penta Sowjanya[1], Balireddy Vasundhara[1], Dasari Kishore Babu[2]

[1]Department of Physics, Gandhi Institute of Technology and Management, Visakhapatnam, India
[2]Department of Physics, Gyeongsang National University, Jinju, Gyeongsangnam do, Republic of korea
Email:spenta2@gitam.in

This study investigates the use of Wavelength Dispersive X-ray Fluorescence (WDXRF) for the analysis and differentiation of Strontium (Sr) and Strontium Nitrate (Sr(NO3)2).
WDXRF spectra revealed unique peaks for each material, with significant differences in their peak height-to-width ratios, which corresponded to varying resolution and structural characteristics. The experimental results showed strong agreement with theoretical values, validating the accuracy of the technique. To improve the precision of peak identification, the moving average technique was applied to reduce noise in the spectra, allowing for more accurate determination of peak locations, heights, and widths.
The study demonstrates that WDXRF is an effective and reliable method for distin- guishing between materials with subtle compositional differences and for providing detailed material characterization.

1. Introduction

Wavelength Dispersive X-ray Fluorescence (WDXRF) is a powerful analytical technique widely used for determining the elemental composition of various materials [1–6]. It operates by measuring the X-ray fluorescence emitted from a sample when it is excited by an incident X-ray beam [1]. The technique is non-destructive, highly precise, and capable of providing detailed information about the composition of both bulk and trace elements in solid, liquid, or powder samples [1,2,7,8]. WDXRF can analyze a broad range of elements, from Beryllium (Be) to Uranium (U) [7–18]. In this study we present elemental analysis of Sr and Sr(NO3)2 using WDXRF.

One of the challenges in WDXRF spectroscopy is the identification and interpretation of spectral features, particularly when analyzing elements with similar atomic numbers or compounds that exhibit overlapping X-ray lines. Strontium (Sr) and Strontium Nitrate (Sr(NO3)2) are such examples. Despite having similar elemental compositions, Sr and Sr(NO3)2 exhibit distinct spec- tral characteristics due to their different molecular structures and bonding environments.

This study focuses on the analysis of Strontium (Sr) and Strontium Nitrate (Sr(NO3)2) using WDXRF, with particular emphasis on the identification and comparison of satellite lines present in their spectra. Satellite lines are secondary peaks that appear in the fluorescence spectra and are valuable for identifying specific chemical environments of the element being analyzed. By comparing the experimental WDXRF spectra of Sr and Sr(NO3)2 with theoretical predictions, this paper aims to demonstrate the capability of WDXRF in distinguishing between these two compounds and providing insights into their molecular structures.

The paper also discusses the processing of the WDXRF data using the moving average technique to reduce noise, as well as the measurement of key spectral parameters such as peak location, height, and width. This comprehensive analysis highlights how WDXRF can be used effectively to resolve subtle differences between chemically similar materials, paving the way for more precise and reliable elemental analysis.

In Section 2, the experimental conditions, method to obtain modified intensity, and data processing tools are discussed. Results and discussion are presented in Section 3. The Section 4, presents conclusions.

2. Methodology

In Section 2.1, the experimental conditions, in Section 2.2, method to obtain modified intensity, and in Section 2.3 data processing tools that are used will be discussed.

2.1 Experimental conditions

In this section, we present details of experimental conditions to collect L-X ray data for Sr and Sr(NO3)2. In order to prepare sample, we took powder specimen of Sr and Sr(NO3)2. The instrument used to collect data is high performance sequential Wavelength Dispersive X-Ray Fluorescence Spectrometer (Model: S8,Tiger,Bruker,Germany) fortified with Rh anode X ray tube (4KW,60KV and 170mA). It has automated sample changer. A gas flow proportional (90% Ar – 10% CH4) detector is used to record low and high characteristic X Ray intensities. These intensities are separated by X Rays based on wavelength by reflectivity through high resolution Poly Ethylene Terephthalate PET (002) (2d=8.7522Ao) crystal. The normal time of every spectrum was nearly 20 minutes. The chemicals are of 99.9% purity. In our work we used the pressed pellet method. In the dia-set firstly filled with high purity cellulose powder about 3 g then surface filled with samples (high purity element powder) about 50 to 10 mg. The sandwich mixer applied 8 tons pressure to bind the sample with cellulose powder to make the 40 mm dia pellet. The thickness of the samples on the 4 mm thick cellulose bed is 200 to 500 μm. [19].

The pellets are mounted on the pellet frame (nearly $3 \times 10{-}3$ torr) and the statistics of L X

Ray emission spectra of Sr and Sr(NO3)2 were verified in energy scan mode of 0.15 seconds of data collection per step. By applying Copper filter bremsstrahlung X Rays coming from X Ray tube is removed and instrumental calibration is checked in routine by regulating the shift of Goniometer. From WDXRF Spectrometer, the counts and intensity (I0(θ), where θ is the angle of diffraction) values collected with the step size of 0.4 eV through the system connected to the instrument.

2.2 Method to obtain energy and modified intensity

In this section, the method for obtaining energy and modified intensity is presented.

The energy in eV is the given by the formula $E = hc/\lambda$, where h is Planck's constant, c is speed of light $\lambda = 2d \sin\theta$ which is equal to wavelength of X-Ray, and θ is the angle of diffraction [20].

The modified intensity is calculated using the formula $I(E) = I0(\theta)\tan\theta$. The range of θ values for I(E) happen to be large, hence the Logarithm of I(E) will be used in plots energy versus modified intensities for Sr and Sr(NO3)2.

2.3 Data processing

In this section, the data processing tools used are discussed.

In order to plot energy versus log(I(E)), plotting function from the Matplotlib library in Python [22, 23] is used. The noise in log(I(E)) is reduced by smoothing using moving average function that is available in NumPy [22]. This function uses simple moving average. The peak heights for smoothed signal are found using find peaks function that is available in SciPy [22]. The half widths are obtained using peak widths function that is available in SciPy [22].

3. Results and discussion

In this section, results and discussion are presented.

The plot shown in Fig. 1 illustrates Energy (E) on the x-axis and the logarithm of intensity (log(I(E))) on the y-axis for Sr and Sr(NO3). From the figure, it is evident that the logarithm of intensity exhibits significant noise for both Sr and Sr(NO3), making it challenging to identify peaks in the data.

To address this issue, the logarithm of intensity was processed using a moving average function implemented in Python. This function applies a smoothing technique that reduces noise while preserving the essential features of the data. The resulting smoothed plot, also shown in Fig. 2, displays Energy on the x-axis and the moving average of log(I(E)) on the y-axis. Compared to the original plot, the smoothed version exhibits significantly less noise, enabling clearer visualization of peaks in the data.

Using the smoothed log(I(E)), peak locations were identified with the help of the find peaks function available in Python. This function detects local maxima in the data, which correspond to the prominent peaks. Additionally, the widths of these peaks were calculated using the peak widths function, also provided in Python. The peak positions and their corresponding half-widths give valuable insights into the spectral properties of Sr and Sr(NO3).

In Fig. 2, the detected peaks are marked with an asterisk (∗) symbol for easy identification. It should be noted that for both Sr and Sr(NO3) the peak locations are are almost same.

The data presented in Tables 1 and 2 corresponds to Sr and Sr(NO3)2, respectively. These tables display the satellite lines, including theoretical values discussed by Gunter Zschornack [1], alongside the observed peak positions (on the x-axis) and their heights.

For both Sr and Sr(NO3)2, the satellite lines Ll(L3M1), Lη(L2M1), Lβ17(L2M3), Lα1(L3M5), Lβ1(L2M5), Lβ6(L3N1), Lβ4(L1M2), Lβ3(L1M3), and Lβ9(L1M5) were observed in the WDXRF spectrum. These satellite lines show good agreement with the theoretically predicted lines dis- cussed in "Handbook of X-Ray Data" by Gunter Zschornack [1].

The Ratio, defined as Peak height indicates the resolution of the peaks. A higher ratio signifies better separation of the peaks.

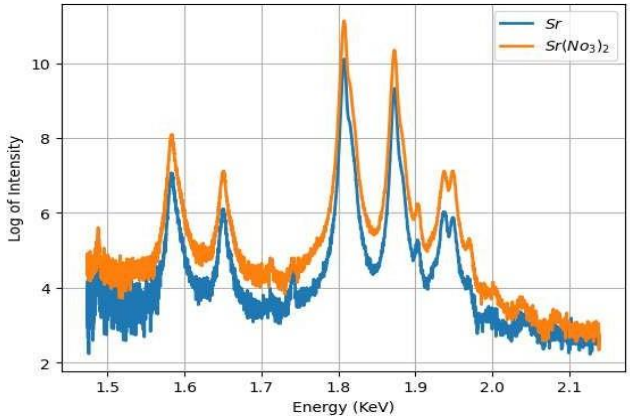

Figure 1: Energy versus log of intensity (log(I(E))) for Sr and Sr(NO3)2.

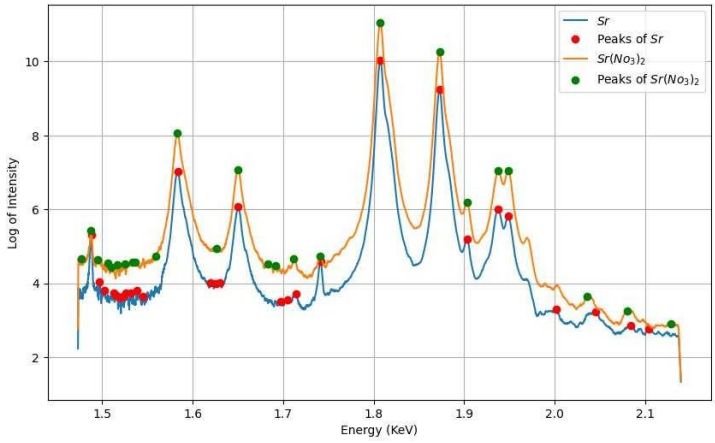

Figure 2: Energy versus moving average of log(I(E)) for Sr and Sr(NO3)2.

From the data presented in Table 1, the peak positions for Sr are observed at: 2.10375009921669, 2.08420261876441, 2.04528558809234, 2.00211727543011,

1.94835614401501, 1.93729740859323,

1.90313191046451, 1.87287644824354, 1.80725546554063, 1.74134737998672, 1.7143720010997,

1.70519623342229, 1.69715986679343, 1.65035332969633, 1.62996948972004, 1.62592674369577,

1.62005248941872, 1.58390237537055, 1.54485909160202, 1.53837439179741, 1.53143510891261,

1.52626236939373, 1.52310126127279, 1.51950281063814, 1.51573662715119, 1.51299553376757,

1.50225546699933, 1.49726555933685, and 1.48799523636024.

From the data shown in Table 2, the peak positions for Sr(NO3)2 are observed at: 2.12830516094607,

Table 1: Location, Height, and Half Width of Peaks for Sr

Satellite Line	Theoretical Value [1]	Peak Location (x-axis)	Peak Height	Peak Width	Ratio = $\frac{\text{Peak Height}}{\text{Peak Width}}$
		1.48799523636024	5.30581581033114	1.86721955628082	2.84155968294346
		1.49726555933685	4.02951478288437	0.869654288482707	4.6334673861204
		1.50225546699933	3.79639366639355	0.101347767395055	37.459075458418
		1.51299553376757	3.72984441494192	0.134172770022815	27.7988180038893
		1.51573662715119	3.67212844094237	0.196092489164584	18.726512456376
		1.51950281063814	3.61142455406777	0.133701618543	27.0110758076297
		1.52310126127279	3.6493982415417	0.375613448908098	9.71583486201157
		1.52626236939373	3.73272680575221	0.104729962581132	35.6414412242394
		1.53143510891261	3.74480842064597	0.547896724994189	6.83488009658332
		1.53837439179741	3.81670777407686	0.283953576027216	13.44130906001
		1.54485909160202	3.65579014440293	1.19877471754262	3.04960564391696
$L_l(L_3M_1)$	1.582174	1.58390237537055	7.0338605060232	11.0474748431807	0.636693960010691
		1.62005248941872	4.00804616616629	0.284567374838843	14.0847002170791
		1.62592674369577	3.99289880894986	0.071851090820246	55.5718606825207
		1.62996948972004	4.01204051457724	0.348334973063402	11.5177654408161
$L_\eta(L_2M_1)$	1.6493	1.65035332969633	6.07722747986585	3.9170139920268	1.55149496331548
		1.69715986679343	3.51440288382447	0.124482284828673	28.2321527811078
		1.70519623342229	3.55831607405332	0.048437751916481	73.4616272074057
		1.7143720010997	3.70972585898361	0.41371235318843	8.96692068871816
$L\beta17(L2M3)$	1.7383	1.74134737998672	4.59522579789441	1.35700572983228	3.38629800661369
$L_{\alpha1}(L_3M_5)$	1.8066	1.80725546554063	10.0350407964461	6.06723740457846	1.65397200196476
$L_{\beta1}(L_2M_5)$	1.87388	1.87287644824354	9.24042879052345	4.46111992673173	2.07132490098582

$L_{\beta6}(L_3N_1)$	1.90183	1.90313191046451	5.20093965877857	0.471170929324899	11.0383288422114
$L\beta4(L_1M_2)$	1.93644	1.93729740859323	5.99710271645109	4.59972197655731	1.30379678315681
$L_{\beta3}(L_1M_3)$	1.94720	1.94835614401501	5.81214564478661	1.83930932167499	3.15996095724329
		2.00211727543011	3.2934145148516	0.110648325424165	29.7647027392999
		2.04528558809234	3.2195747845055	1.24556611152187	2.58482850064999
$L_{\beta9}(L_1M_5)$	2.0822	2.08420261876441	2.85751073529823	0.195785208137551	14.5951308706154
		2.10375009921669	2.76495305470783	0.159769758334988	17.3058599044168

2.0804485645988, 2.03555267343751, 1.94835614401501, 1.93767546623813, 1.90313191046451,

1.87287644824354, 1.80725546554063, 1.74108727568661, 1.7119372426182, 1.69135343684124,

1.68291675855706, 1.65014734333453, 1.62688462893676, 1.58324185677486, 1.55904721169686,

1.53675125137069, 1.53341173824424, 1.52486471591808, 1.51682152585954, 1.51053200021927,

1.5068493604815, 1.49535970631981, 1.48789584100426, and 1.47716428990867

It is noteworthy that the following peaks are unique to Sr: 2.10375009921669, 2.00211727543011, 1.70519623342229, 1.62592674369577, 1.62005248941872, 1.54485909160202, 1.51299553376757,

1.52310126127279 The corresponding peak height-to-width ratios for these unique peaks are: 17.3058599044168, 29.7647027392999, 73.4616272074057, 55.5718606825207, 14.0847002170791,

3.04960564391696, 13.44130906001, 9.71583486201157, respectively.

Similarly, the following peaks are unique to Sr(NO3)2: 2.12830516094607, 1.68291675855706, 1.55904721169686, 1.47716428990867 are unique to Sr(NO3)2. The corresponding peak height-to- width ratios for these unique peaks are: 23.4433385287741, 32.7418859627105, 6.16339545009855, 31.75622204697, respectively.

In conclusion, the WDXRF analysis effectively distinguishes subtle differences between Sr and Sr(NO3)2, particularly through the identification of unique peak positions and their corresponding height-to-width ratios.

Table 2: Location, Height, and Half Width of Peaks for Sr(NO3)2

Satellite Line	Theoretical Value [1]	Peak Location (x-axis)	Peak Height	Peak Width	Ratio = $\frac{\text{Peak Height}}{\text{Peak Width}}$
		1.47716428990867	4.65258401734266	0.146509367848012	31.75622204697
		1.48789584100426	5.4161830797127	1.94580919231976	2.78351191940646
		1.49535970631981	4.64942016199137	1.20581045020344	3.85584663095839
		1.5068493604815	4.54297621261109	0.234442348389166	19.3777969032707
		1.51053200021927	4.43982012510701	0.13235303211286	33.5452845637951
		1.51682152585954	4.49054611026184	0.746137505760998	6.0183894732404
		1.52486471591808	4.52320887121256	0.504780031879363	8.96075237836182
		1.53341173824424	4.57889627326727	0.184893282225857	24.7650764708363
		1.53675125137069	4.5783650286977	0.123544285828757	37.0584928148252
		1.55904721169686	4.72704929163994	0.766955378721377	6.16339545009855

$L_l(L_3M_1)$	1.582174	1.58324185677486	8.06096464166779	8.84826177014247	0.911022396383962
		1.62688462893676	4.9446631949636	0.087201215159666	56.7040629641441
$L_\eta(L_2M_1)$	1.6493	1.65014734333453	7.08152509299587	6.65568813513505	1.06398090613844
		1.68291675855706	4.51971957664603	0.138040905212165	32.7418859627105
		1.69135343684124	4.47136582861393	0.227948728612546	19.6156646971877
		1.7119372426182	4.67112051343113	1.24572128407431	3.74973163993279
Lβ17(L2M3)	1.7383	1.74108727568661	4.72303505904352	0.754351373516784	6.2610544964275
$L_{\alpha1}(L_3M_5)$	1.8066	1.80725546554063	11.0598406739805	6.49378168718567	1.70314328487591
$L_{\beta1}(L_2M_5)$	1.87388	1.87287644824354	10.2669024572155	4.69376430517718	2.18734938307218
$L_{\beta6}(L_3N_1)$	1.90183	1.90313191046451	6.20193457293718	0.825941084966985	7.50893094655182
$L_{\beta4}(L_1M_2)$	1.93644	1.93767546623813	7.05818558029997	4.46027285059279	1.5824560103676
$L_{\beta3}(L_1M_3)$	1.94720	1.94835614401501	7.05601454232051	1.75021064027976	4.03152305210111
		2.03555267343751	3.63437109549043	0.487632719752952	7.45309112426192
Lβ10(L1M4)	2.0805	2.0804485645988	3.24953930772811	0.269691770070622	12.049085913438
		2.12830516094607	2.89947651259782	0.123680187829862	23.4433385287741

4. Conclusions

In this study, Wavelength Dispersive X-ray Fluorescence (WDXRF) was employed to analyze Strontium (Sr) and Strontium Nitrate (Sr(NO3)2). The data obtained from WDXRF revealed several unique peaks for each material, with noticeable differences in their respective peak height- to-width ratios. These differences were particularly pronounced in the satellite lines, which pro- vided clear evidence of the varying structural characteristics of Sr and Sr(NO3)2. The higher peak height-to-width ratios observed for certain peaks in Sr(NO3)2 suggest a higher resolution, indicating distinct material properties.

The experimental results showed a strong correlation with the theoretical values discussed in"Handbook of X-Ray Data" by Gunter Zschornack [1], confirming the accuracy and reliability of the WDXRF technique. This agreement between experimental and theoretical data further validates the use of WDXRF for detailed material characterization and spectral analysis.

Additionally, the study employed a moving average technique to reduce noise in the spectra, enhancing the precision in determining peak locations, peak heights, and peak widths. This noise reduction method improved the clarity of the spectral data, ensuring that the observed peaks were accurately represented and analyzed.

References

1. Gunter Zschornack. Handbook of X-Ray Data. Springer-Verlag Berlin Heidelberg, 2007.
2. J. A. Bearden. X-ray wavelengths. Reviews of Modern Physics, 39(1), 1967.
3. Ellery Storm and Harvey L. Isreal. Photon cross sections from 1 kev to 100 mev for elements z=1 to

z=100. Nuclear Data Tables, A7:565–681, 1970.
4. M. Guerra, P. Amaro, J. P. Santos, and P. Indelicato. Relativistic calculations of screening parameters and atomic radii of neutral atoms. Atomic Data and Nuclear Data Tables, 2017.
5. Takeshi Mukoyama and Kazuo Tanguchi. Atomic excitation as a result of inner shell vacancy production. Physical Review A, 36(2), 1987.
6. Thomas A. Carlson, C. W. Nestor Jr.and Thomas C. Trucker, and F. B. Malik. Calculation of electron shake off for elements from Z=2 to Z=92 with the use of self-consistent field wavefunctions. Physical Review, 169(1), 1967.
7. Harpreet Singh Kainth. Structure of high resolution Lα, Lβ1 x-ray emission spectra of 38sr compounds. Journal of Alloys and Compounds, 782:404–412, 2019.
8. G. D. O'Kelley, R. L. Auble, L. D. Hulett Jr., H. J. Kim, W. T. Milner, S. Raman, O. Shahal,
9. C. R. Vane, J. P. Young, and G. Lapicki. Implications of heavy ion induced satellite X-ray emission ii production of k and l x rays by 0.9 to 2.6 mev/u argon ions in thick targets of vanadium, copper, niobium, tantalum, and platinum. Nuclear Instruments and Methods in Physics Research, B3:78–87, 1984.
10. Omer Sogut, Erdogan Buyukkasap, Mehmet Erutugrul, and Adnan Kucukonder. Chemical effect on L X-ray intensity ratios of mercury, lead, bismuth. Applied Spectroscopy Reviews, 32(1–2):167–173, 2006.
11. H. R. Verma. Measurements of M and L X-ray energies and relative intensities emanating from 241am source. Applied Radiation and Isotopes, 122:41–46, 2017.
12. Xing Wang, Zhongfeng Xu, and Limin Zhang. L X-ray intensity ratios for high Z elements induced with X-ray tube. Radiation Physics and Chemistry, 112:121–124, 2015.
13. C. Aksoy, E. Tirasoglu, E. Cengiz, G. Apaydin, M. Saydam, V. Aylicki, and N. K. Aycli. Chemical effects on the L shell X-ray fluorescence parameters of ta and w compounds. Journal of Electron Spectroscopy and Related Phenomenon, 184:556–560, 2011.
14. Malte Wansleben, Yves Kayser, Philipp Honike, Ina Holfelder, Andre Wahlisch, Rainer Unterumsberger, and Burkhard Beckhoff. Experimental determination of line energies, line widths, and relative transition probabilities of gadolinium L X-ray emission spectrum. arXiv preprint, arXiv:1903.08085, 2019.
15. J. Xu and E. Rosato. Relative intensities of diagram and satellite L X-rays for elements Z=37 to 56. Journal de Physique Colloques, 48:C8–661–C8–664, 1987.
16. M. Czarnota, M. Pajek, D. Danas, D. Chmielewska, J. Rzadkiewicz, Z. Sujkowski, J.-Cl. Dousse, M. Berset, O. Mauron, Y.-P. Maillard, P. A. Raboud, J. Hoszowska, M. Polasik, and
17. K. Slabkowska. Observation of L X-ray satellites and hypersatellites in collisions of o and ne ions with mo and pd. Nuclear Instruments and Methods in Physics Research, B205:133–138, 2003.
18. Yu Liu, Jhong Feng Xu, Xing Wang, and Lixia Zeng. Angular dependence of ag L X-rays emission induced by 20 to 40 kev electron impact. Nuclear Instruments and Methods in Physics Research, B446:1–4, 2019.
19. Harpreet Singh Kainth, Ranjith Singh, Gurjot Singh, and D. Mehta. Chemical shifting of Lα, Lβ1 , Lβ3,4 , Lβ2,1,5 , Lγ1 , Lγ2,3 emission lines of 47ag, 48cd, 50sn compounds. Nuclear Instruments and Methods in Physics Research, D141:84–98, 2018.
20. R. Yilmaz. Kβ/Kα X-ray intensity ratios for some elements in the atomic number range $28 \leq z \leq 39$ at 16.896 kev. Journal of Radiation Research and Applied Sciences, 10(3):172– 177, 2017.
21. P. Sowjanya, B. Vasundhara, and D. Kishore Babu. Determination of L X-ray satellite tran- sitions of hg compound. In Proceedings of International Conference on Advances in Materials and Processing Challenges and Opportunities, 2022.
22. Neil W. Ashcroft and N. David Mermin. Solid State Physics. Harcourt, Orlando, 1976.
23. Akihiko Iwata, Koretaka Yuge, and Jun Kawai. Intensity correction of wd-xrf spectra from 2θ to energy. X-Ray Spectrometry, 42(1):16–18, 2013.
24. Python Software Foundation. Python Language Reference, version 3.x, 2023.
25. John D. Hunter. Matplotlib: A 2d graphics environment. Computing in Science & Engineer- ing, 9(3):90–95, 2007.